nature energy

REVIEW ARTICLE

PUBLISHED: 29 FEBRUARY 2016 | ARTICLE NUMBER: 16016 | DOI: 10.1038/NENERGY.2016.16

Colloidal quantum dot solids for solution-processed solar cells

Mingjian Yuan†, Mengxia Liu† and Edward H. Sargent*

Solution-processed photovoltaic technologies represent a promising way to reduce the cost and increase the efficiency of solar energy harvesting. Among these, colloidal semiconductor quantum dot photovoltaics have the advantage of a spectrally tuneable infrared bandgap, which enables use in multi-junction cells, as well as the benefit of generating and harvesting multiple charge carrier pairs per absorbed photon. Here we review recent progress in colloidal quantum dot photovoltaics, focusing on three fronts. First, we examine strategies to manage the abundant surfaces of quantum dots, strategies that have led to progress in the removal of electronic trap states. Second, we consider new device architectures that have improved device performance to certified efficiencies of 10.6%. Third, we focus on progress in solution-phase chemical processing, such as spray-coating and centrifugal casting, which has led to the demonstration of manufacturing-ready process technologies.

Photovoltaic devices generate electricity directly from solar radiation, which is abundant and freely accessible, offering the potential for renewable power on a vast scale. Worldwide photovoltaic production will exceed 40 GW in 2016 and the overall solar market will exceed US$80 billion in revenues[1]. Continued reductions in the cost of solar electricity production, including via reductions in the capital costs associated with solar cell and module manufacture, remain a priority for the sector.

Solution-processed photovoltaics use low manufacturing temperatures, and have consequently minimized energy expenditure, in their fabrication. Among solution-processed solar technologies, colloidal quantum dots (CQDs) are actively explored, particularly for their spectral tunability at the time of synthesis. Through the quantum size effect, the bandgap of quantum dot solids is readily tuned at the point of manufacture, offering avenues to tandem and multi-junction solar cells that improve utilization of the broadband solar spectrum (Fig. 1) compared with single-junction cells. CQD photovoltaics offer the opportunity to reduce thermalization losses: multiple exciton generation, as well as the prospect of photon up- and down-conversion, have the potential to further improve spectral utilization.

The performance of CQD photovoltaic devices has increased in the past decade to certified power conversion efficiencies (PCEs) of 10.6% in 2015[2]. Here we review advances that have enabled this progress and we discuss further innovations that are required to make CQD photovoltaics a commercially compelling technology. Three key areas in particular have seen major strides in recent years, and these represent the three focal areas of this Review. Researchers have demonstrated enhanced control over the electronic properties of CQD solids, and these have led directly to improved solar cell performance. At the level of device architecture, the community has realized numerous forms of grading in electronic levels throughout the thickness of the active layer, enabling devices that guide electrons or holes efficiently towards their respective charge-collecting contacts. Finally, the full value of solution-processed film deposition is closer at hand with new solution-phase chemistry that allows direct deposition of CQD inks to form the desired solids in a single, straightforward fabrication step.

Surface chemistry determines the electronic properties

Each CQD — comprising hundreds to thousands of atoms — can be viewed as an artificial atom providing, through its size and shape, a series of energy levels analogous to the orbital energy levels of actual atoms. The assembly of constituent atoms is imperfect, and CQDs are not absolutely identical to one another in the number and arrangement of atoms. In addition, defects and impurities within the crystal and its surface influence its optoelectronic properties. As a result, undesired electronic states lie well within the bandgap of the CQD solid (Fig. 2a,b). This population of midgap states limits the performance of CQD solids, and progress in removing these states has been a priority both for materials processing and solar performance during the past five years.

In early research on CQD solids, lack of fundamental understanding of the origins of midgap state formation stood in the way of their removal. Recently, understanding of the origins of these midgap states has been considerably deepened. In lead chalcogenide PbX (X = S, Se) CQDs — materials that are particularly prominent in CQD photovoltaics in view of their wide-size-tuned bandgap arising from a large Bohr exciton radius — multiple distinct facets are exposed at the CQD surface. The facets' relative contributions depend on particle size and synthetic conditions. Of particular interest are the polar (111) and nonpolar (100) crystalline planes, which are the dominant facets, each of which has a distinct character[3]. As-prepared PbX CQDs are significantly off-stoichiometric and lead-rich, with the excess Pb atoms located on the Pb-terminated (111) surface[3–5]. Overall charge balance is maintained by undercharging of the Pb atoms, producing off-stoichiometry that can be a major cause of midgap states[6]. Traps emerge even when the system is only minimally off-stoichiometric ($Pb_{63}S_{62}$). Visualization of the wave function distribution reveals states whose wave functions are localized to the surface. In contrast, precisely stoichiometric CQDs are devoid of midgap states and retain this quality independent of CQD shape[7]. Analogously, in PbSe, dangling Se and Pb bonds are responsible for states inside the bandgap[8]. Oxygen-related species on the CQD surface are another cause of midgap states, an insight that motivated the successful application of hydrazine, a strong reducing agent, leading to an appreciably cleaner bandgap and a Fermi

Department of Electrical and Computer Engineering, University of Toronto, 10 King's College Road, Toronto, Ontario M5S 3G4, Canada. †These authors contributed equally to this work. *e-mail: ted.sargent@utoronto.ca

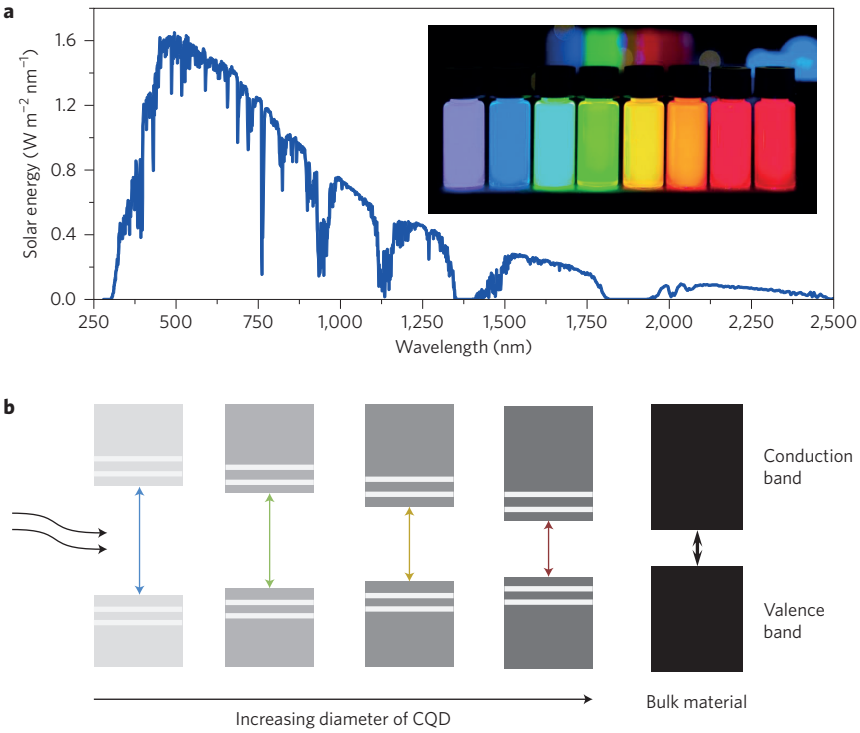

Figure 1 | Advantages of CQD solids. a, Nanoparticle-size-dependent absorption enables tuning of the CQD absorption spectrum. The insert shows photoluminescence of CQDs with different particle sizes. **b**, Conduction and valence band energy levels also benefit from control via ligand adsorption and stoichiometry.

level near the midgap[9]. Previous studies showing dramatic increases in charge carrier mobility in hydrazine-treated lead chalcogenide CQDs may also have benefited from midgap state removal[10].

Midgap states play an essential role in charge transport, especially when the diffusion of excitons or minority carriers represents the dominant transport mode. Traps decrease both the effective carrier mobility and the excited state lifetime[11], the latter owing to their role as recombination centres (Fig. 2c). The average spacing among deep recombination centres limits the diffusion length of excited photocarriers in present-day CQD films[12], for the diode current is dominated by trap-assisted recombination[13]. By pinning the Fermi level at least 0.1 eV and as much as 0.4 eV (ref. 13) below the conduction band edge, midgap states cause an appreciable deficit in open-circuit voltage (V_{oc}) seen in CQD photovoltaics[14]. Further reducing midgap states should increase the diffusion length, reduce recombination and trapping, and enable continued advances in PCE[15].

Fundamental studies of midgap states have provided important guidance to the community, with direct recent observations coming from scanning tunnelling spectroscopy measurements. The midgap band was found to be substantially invariant with particle size[16], again confirming the role of surface chemistry on the atomic scale over that of electronic states delocalized across the multinanometre dimensions of the particles. Spectrally resolved studies of a gate-voltage-dependent photocurrent in optical field-effect transistors also revealed midgap states that can form a weakly conducting band[17]. Recently, efforts to quantify trap states experimentally have exploited deep-level transient spectroscopy[18], thermal admittance spectroscopy[11], Fourier transform photocurrent spectroscopy[11] and scanning tunnelling spectroscopy[16]. Midgap states with densities in the range of 10^{16}–10^{17} cm^{-3} have been identified through these complementary measurement techniques.

Efforts to balance the stoichiometry of the CQD surface to eliminate the midgap states have been pursued, including through the introduction of a small quantity of excess Pb (1–10 Å equivalent thickness) and Se (0.1–10 Å) via thermal evaporation[19]. This strategy enabled precise tuning of carrier statistics via stoichiometric control. The deposition of excess Pb rendered the film n-type, whereas the deposition of extra Se produced p-type behaviour. This agrees well with observations in bulk lead chalcogenides[20]. Balanced stoichiometry is also pursued through solution-phase metal salt treatments, which have been shown to improve carrier mobility and lifetime[21]. High-performance unipolar n- and p-type nanocrystal-based field-effect transistors, as well as solar cells with increased performance, are obtained through this strategy.

An effective method to reduce midgap traps in PbSe CQDs was recently reported based on post-synthetic treatment using molecular chlorine (Cl_2)[22]. Cl_2 preferentially etches surface Se atoms and reacts with Pb atoms to form a thin (1–2 atomic monolayer) $PbCl_x$ passivation layer. The resulting CQD solution exhibits strikingly enhanced photoluminescence quantum yield and reduced photocharging. Very recently, a solution-based passivation scheme was developed that employed molecular iodine (I_2) and PbS CQDs. A very thin PbI_2 passivation layer was formed as a result of I_2 treatment and this produced a twofold decrease in trap states density that improved the photocarrier diffusion length. Ultimately this advance led to a certified PCE of 9.9%[23].

Increasing the density, and thus the completeness, of surface ligand coverage represents an additional means of reducing midgap states (Fig. 2d). Short organic ligands were investigated in light of their potential to increase the surface coverage during ligand exchange[24,25]. However, density functional theory simulations indicated that steric hindrance prevents organic ligands from penetrating the inter-cation trenches on the surface of CQDs, and that this can lead to incomplete passivation of surfaces. A hybrid passivation scheme was therefore developed, one that utilizes halide anions during the end stage of synthesis[26]: the halide atom is sufficiently compact to bind sites inaccessible to typical organic ligands. In these studies, a range of metal cations was introduced to bind unpassivated surface chalcogens, simultaneously mitigating valence-band-associated trap states[27].

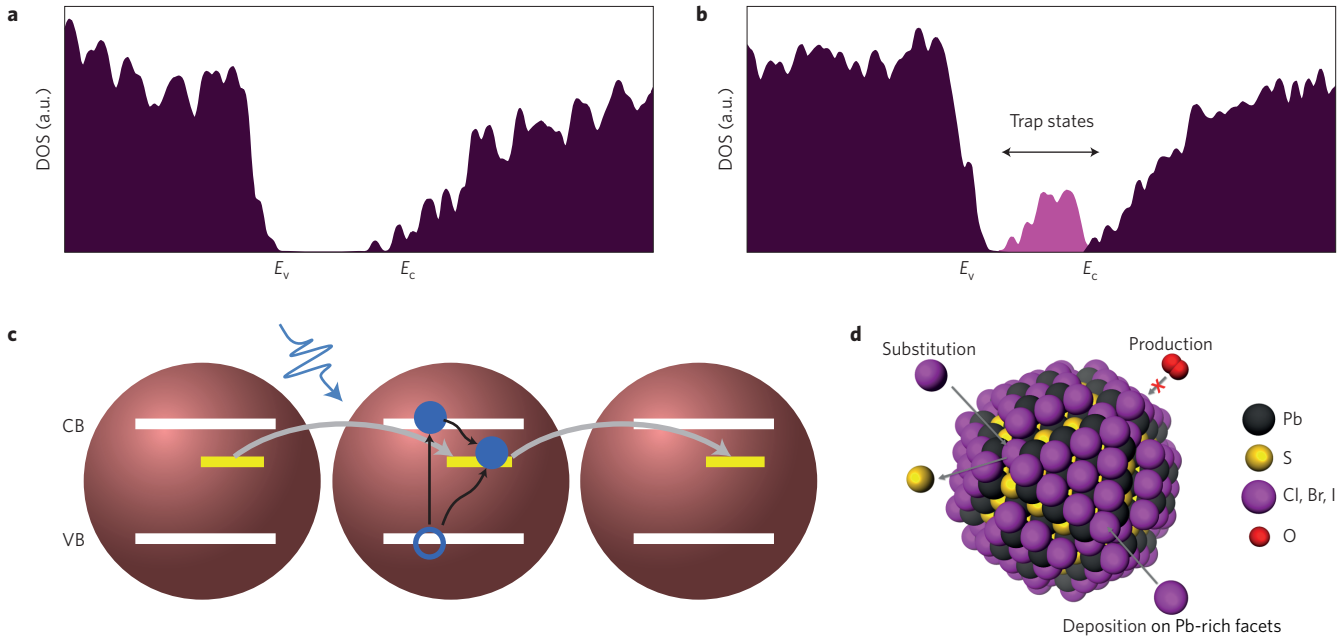

Figure 2 | Advances in purifying the bandgap of CQD solids. a,**b**, Density of states (DOS) showing a scenario with a clean bandgap (**a**) versus a solid that suffers from midgap states (**b**). E_v is the energy level of the top of the valence band and E_c is the energy level of the bottom of the conduction band. **c**, Midgap states (yellow) function as recombination centres, capturing both electrons (blue spheres) and holes (blue circles) with similar probabilities, and enabling their loss through recombination. VB, valence band; CB, conduction band; wavy arrow represents incoming photons. **d**, Effective surface passivation seeks to eliminate electronic states within the bandgap. Figure reproduced from: **a**,**b**, ref. 26, NPG; **c**, ref. 17, NPG; **d**, ref. 55, Wiley.

Recently, an atomic ligand passivation scheme was introduced that entirely displaced organic ligands, replacing them with inorganic passivants based on atomic halide anions (Cl^-, Br^- and I^-)[28]. Monovalent halide ligands possess small size and strong affinity to cations on the CQD surface, offering strong X-type bonding for highly effective passivation. The use of halide ligands was found, through time-resolved infrared spectroscopy, to reduce the density of midgap states, further contributing to increased electron mobility. Transient photovoltage and thermal admittance spectroscopies were used to obtain the midgap trap state density in the hybrid passivated films. The density was found to be 2×10^{16} cm^{-3} eV^{-1}, five times lower than in conventional organic-crosslinked films[26].

These halide passivation schemes were realized via a solid-state ligand exchange, one in which the CQD solids are first assembled into a densely packed thin film, then soaked using a solution that introduces the additional passivants. In this process, steric hindrance can prevent the complete replacement of bulky organic ligands, and may even limit access to the surface by the halide anions. With this in mind, researchers further improved halide treatments by adding halide precursors in the solution phase during synthesis and, in related separate studies, by replacing organic ligands in the solution phase using phase-transfer techniques. The approach enabled a more complete ligand exchange and reduced volume contractions during subsequent film processing. Tetrabutylammonium halide[29], methylammonium halide[30], lead halide perovskite[31,32], and pseudohalide and halometallate ligands[31] have been used in solution to passivate CQD surfaces. The strategy has been applied to PbSe[33], CdTe[34] and CdSe[35,36] nanocrystal films, improving field-effect transistors and solar cells alike.

Programmable CQDs enable graded-architecture devices

CQD photovoltaic devices rely on the judicious engineering of conduction and valence band energy levels among their absorber and charge-extracting layers. This is the basis both of homojunctions (which leverage the ability to dope n-type versus p-type) and heterojunctions (wherein a band offset creates conditions for charge separation based on misaligned energy levels). As the energy levels of inorganic interfaces have been previously successfully tuned by grafting dipolar organic molecules onto surfaces, one would expect that the highest occupied molecular orbital and lowest unoccupied molecular orbital levels relative to vacuum can be engineered in coupled CQD solids through modification of CQD surface ligands.

Through the use of photoelectron spectroscopy in air and ultraviolet photoelectron spectroscopy, researchers saw significant shifts in band energy levels on a variety of organic and inorganic ligand-capped CQDs[37]. The bandgap remained relatively unchanged on ligand adsorption, but the positions relative to vacuum of the valence band maximum and conduction band minimum were shifted appreciably (Fig. 3a). These band edge shifts were concluded to be electrostatic in origin, and to include contributions from both the dipole formed between the surface atom of the CQDs and the binding group of the ligand[38], and the intrinsic dipole moment of the ligand itself[39]. Similar phenomena have also been observed in the CdSe CQD[40] and PbSe CQD[41] systems.

Surface composition has also been seen to play an important role in control over the density of free carriers: both the doping type (p-type versus n-type) and doping magnitude (free carrier density) of CQD solids have been modulated. Ligands absorbed on the CQD surface, or substituted into the CQD lattice, change the stoichiometry of the CQD solids and donate electrons or holes to neutralize unbalanced cations and anions in the system. Several approaches to the doping of CQDs have been demonstrated in multiple materials systems. Dopants can be incorporated into the CQD core by replacing lattice atoms, as in conventional semiconductor doping: n-type net doping was accomplished through incorporation of Cd in InAs CQDs[42], and intrinsic and p-type doping via inclusion of same-valency cations and silver ions, respectively[43]. CdSe CQDs were p-doped with the introduction of silver ions[44] and n-doped by indium diffusion[45]. The analogous doping process can also be accomplished by the use of bound ligands such as thiols[46] and halides[47] that dope via a charge transfer process[18]. These remote-doping processes are explained within a charge–orbital balance

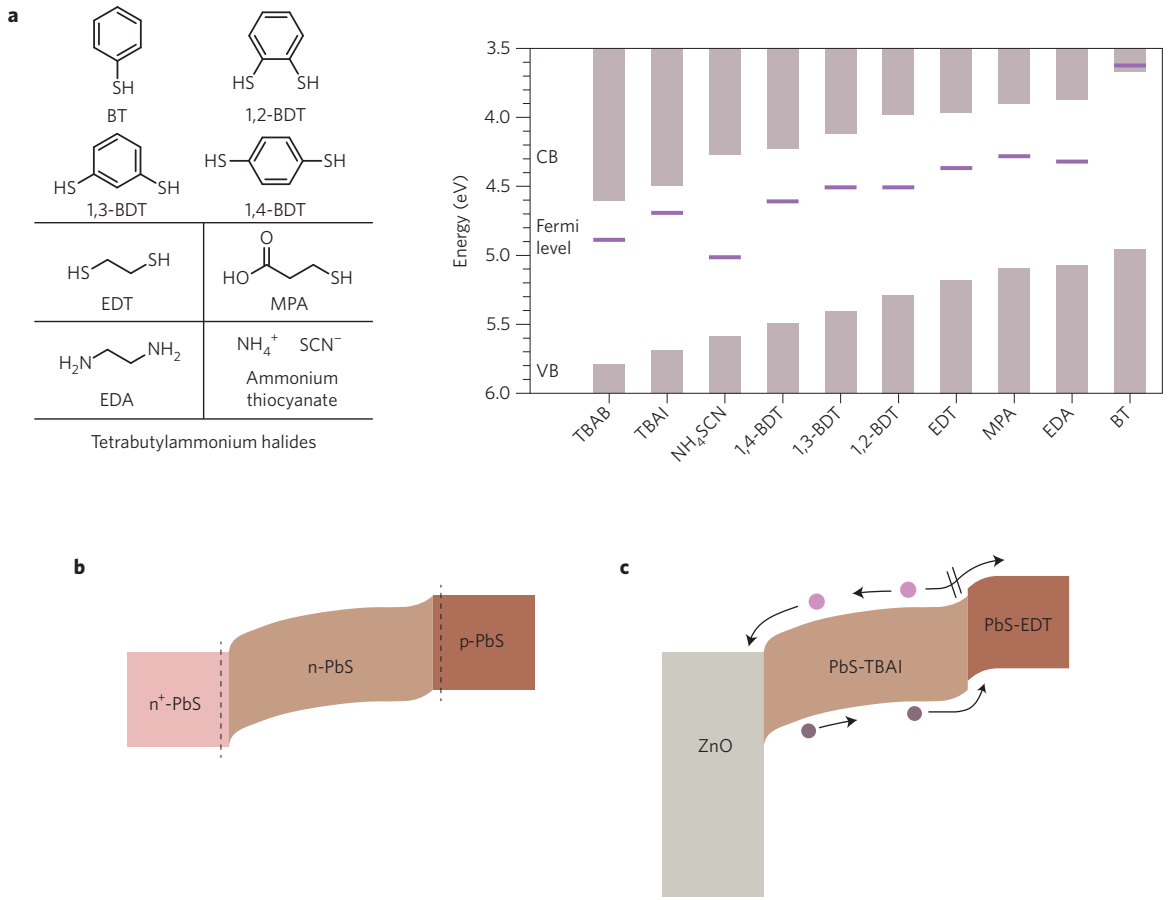

Figure 3 | Band edge control via ligands and stoichiometry. a, Energy levels of PbS CQDs for various different choices of surface ligands. TBAB, tetrabutylammonium bromide; TBAI, tetrabutylammonium iodide; BDT, benzenedithiol; EDT, ethanedithiol; MPA, mercaptopropionic; EDA, ethylenediamine; and BT, benzenethiol. **b**,**c**, Spatial band diagrams for quantum junction devices (**b**) and heterojunction photovoltaic devices (**c**). The conduction band offset between the PbS–TBAI and PbS–EDT layers provides an energy barrier that prevents photogenerated electrons (pink circles) from flowing to the PbS–EDT layer. The brown circles represent photogenerated holes. Figure reproduced from: **a**, ref. 37, American Chemical Society; **c**, ref. 73, NPG.

picture[48]: surface ligands transfer charge from their highest occupied molecular orbital to the conduction band of the CQDs[48,49]. An analogous process can take place from the valence band of CQDs to the surface ligands. Notably, the same dopants can act as either p- or n-dopants, depending on whether they are adsorbed on, or alternatively substituted into, the lattice.

Metal–chalcogen binary compound semiconductors are prone to be n-type when off-stoichiometric with a metal cation excess[50]. To preserve their n-type character, it is important to protect the nanocrystal surface from oxidative attack. However, in an inert ambient environment, widely employed organic ligands such as thiols fail to produce the desired n-type behaviour, instead providing ambipolar characteristics[51]. These sterically large ligands fail to pack densely and thus are unable to ward off oxidative attack even at low oxygen level. Trace oxygen induces Fermi level pinning near the midgap, preventing substantial net doping[52].

Recently, this limitation to the realization of diverse classes of p–n CQD devices was overcome in reports of air-stable n-type CQD films. The use of strongly bound halide ligands was proposed to construct a complete halide ligand shell that would protect the surface of CQDs from direct attack by oxygen and thereby achieve air-stable n-type materials[53]. In particular, iodide ligands conferred superior protection from oxidation through stronger surface binding affinity and little steric hindrance[54,55]. The resultant new materials were used to produce air-processed inverted quantum junction devices, which showed the highest current densities reported from CQD solar cells to that time and a PCE of 8%.

Many advances in CQD solar cells have been featured within the depleted-heterojunction architecture[56], wherein a wide-bandgap n-type bulk material (typically a metal oxide such as TiO_2 or ZnO) is contacted to a p-type CQD film[57]. This architecture, when studied using capacitance–voltage analysis, enabled determination of the role of the depletion region (which provides a built-in electric field beneficial to charge extraction) compared with the role of the undepleted quasi-neutral region, in which photogenerated carriers must rely on diffusion for transport. To date, the sum of the depletion region thickness and the diffusion length — the thickness over which charges are efficiently extracted — is less than the absorption length near the band edge of the CQD solid[58,59]. New classes of structured electrodes have therefore been developed with the goal of enhancing photocharge extraction[60–63].

A further challenge in depleted-heterojunction device engineering has been the requirement of a carefully optimized conduction band offset between the quantum-size-tuned CQD solid and the electron-accepting electrode. This requires, when the CQD solid is redesigned, the electron acceptor to also be re-optimized to achieve efficient carrier extraction without undue loss to open-circuit voltage[64]. The quantum junction architecture (Fig. 3b), in which both sides of the junction, p- and n-, comprised CQD solids, was explored with the goal of overcoming this challenge. Efficient collection was preserved as the CQD bandgap was widely tuned. Photocurrent generation on each side of the junction (in contrast to the depleted heterojunction, in which the n-side is transparent) contributed to enhanced photocurrent. Taking these factors together,

the quantum junction paves straightforward avenues to tandem and multi-junction cells[65]. Early quantum junction devices employed halide-treated PbS CQD layers as the n-type film and used tetramethylammonium hydroxide, a strongly oxidizing agent, for p-type film fabrication[47]. Incorporating silver ions increased doping density in the p-layer, allowing the devices to reach a PCE exceeding 6%[66]. *In situ* Bi-doping was recently employed to convert p-doped PbS CQDs into n-type semiconductors, and a homojunction photovoltaic device that is robust under ambient conditions was thereby achieved[67].

Inspired by the success of bulk heterojunction organic photovoltaics, CQD researchers recently created nano-heterojunction devices constructed by interpenetrating two different nanoparticle-based solids. A large-area charge-separating interface between the n- and p-type solids reduces the requirement for charges to travel long distances before they are separated into electron- or hole-only phases. The most promising of these advances mixed n-type Bi_2S_3 particles with p-type PbS CQDs[68] and, as a result, showed a prolonged carrier lifetime compared with its bilayer counterpart[69]. The result was a threefold improvement in PCE relative to planar controls. Analogously, ZnO nanocrystals as the n-type material have been combined with PbS CQD solids, and an intriguing phenomenon of remote passivation of the CQDs reported. The result was an improved open-circuit voltage (by ×1.25, a very notable augmentation for a V_{oc} value) compared with bilayer devices[70].

Towards the goal of progressive grading in band edge levels, graded n^+–n–p and n–p–p^+ structures have each been developed. For the n^+–n–p structure, distinct halide treatments were employed to fabricate the heavily doped n^+-layer (tetrabutylammonium iodide (TBAI) treated) followed by a more lightly doped n-layer (tetrabutylammonium bromide treated), whereas the p-type layer utilized ligand exchange with tetramethylammonium hydroxide solution[71]. This graded quantum junction architecture showed an increased open-circuit voltage compared with the undoped case, an improvement attributed to the increased built-in voltage offered by addition of the n^+-layer. Analogously, the n–p–p^+ heterojunction devices[72] using 3-mercaptobutyric acid (3MBA), a bidentate ligand, whose lowered packing of ligands on the surface of dots enabled an engineered decrease in doping density. As an added benefit, the bulky branched chain of 3MBA protected the CQDs against oxidation. The resultant well-passivated p-type CQD film exhibited a lower doping level compared with the p^+-mercaptopropionic (MPA)-treated film and enabled a graded architecture exhibiting a PCE of 7.2%.

A feature widely employed in conventional solar cells — an electron-blocking back-surface field — was recently implemented in novel fashion in CQD solids. A p-type layer with a high conduction bandedge introduced a barrier to electrons between the n-type active layer and the hole-accepting contact (Fig. 3c). Implementations relied on TBAI-treated n-type CQD solids augmented by a p-type 1,2-ethanedithiol (EDT)-treated layer on top[73]. The EDT layer blocked electron flow and also enhanced hole extraction from the principal n-type active layer. The reduced electron loss contributed to an improved photocurrent and an enhanced PCE of 8.55%. PbS–EDT layers took the place of the MoO_3 interlayer previously employed in CQD solar cells, providing a direct ohmic contact to gold. This extended the device operating lifetime and led to a remarkable level of stability, with the device left unencapsulated in room air.

New materials processing strategies and combinations

Among the most promising frontiers in CQD photovoltaics is the demonstration of new, commercially relevant manufacturing technologies. Capping ligands play an important role in functionalizing CQDs and are key to ensuring their size-dependent behaviour. However, the insulating nature of long-chain organic ligands limits inter-particle charge transport. As discussed in the preceding two sections, the inter-particle spacing is engineered via a solid-state place exchange to short, conduction-compatible ligands. This place exchange has, to date, largely been practised as a multi-step sequential layer-by-layer process that is wasteful of quantum dots and of solvents, and is incompatible with roll-to-roll manufacturing techniques.

There is therefore intense interest in developing semiconductor inks that enable deposition, over large areas, of the final intended CQD films, and do so in a single processing step. In this vein, solution-phase ligand exchanges have recently been developed in which the native insulating organic ligands are replaced with short inorganic ones in a two-phase solution-exchange procedure. The inorganic ligands provide colloidal stability — specifically in polar solvents — and continue to serve the much-needed goal of surface state passivation. Recent advances have exploited transfer of CQDs across a phase boundary between two immiscible solutions[74]. CQDs transfer into the polar phase and leave behind a colourless nonpolar phase that contains the original organic ligands, to be discarded. Inorganic ligands (S^{2-}) have been shown to bind the CQD surface and introduce a net negative charge, producing an electrostatically stabilized colloid. Counter cations (K^+) do not bind to the CQD surface but do produce an ionic double layer surrounding the CQDs that maintains overall charge neutrality. Different chalcogenides (Se^{2-} and Te^{2-}), hydrochalcogenides (HS^-, HSe^- and HTe^-) and mixed chalcogenides (TeS_3^{2-}) have all been reported[75]. In addition, efficient and flexible CdSe nanocrystal-based field-effect transistors were reported based on an SCN^--capped CQD ink[76].

Molecular metal chalcogenide complexes (MCCs) such as AsS^{3-}, $Sn_2S_6^{4-}$ and $In_2Se_4^{2-}$ have also been used to replace the original organic ligands and stabilize the CQD solution in various polar media. Here, the positive counter cations[77] were Na^+, K^+ and $N_2H_5^+$. The terminal chalcogenide atoms of MCC ligands have strong affinity to under-coordinated and electron-deficient metal atoms on the CQD surface[78]. The MCC-capped CQDs exhibit sufficiently short inter-particle distance to produce efficient electronic coupling between neighbouring CQDs. Quantum dot solids exhibiting impressive electrical conductivities and electron mobilities have been achieved using these MCC-enabled CQD inks[79].

Even with these major advances in MCCs, it remained an open problem to produce high-efficiency photovoltaics using CQD inks. Recently, iodide ligands, with their strong binding affinity to the surface of PbS CQDs[80], were investigated. Progress with iodide salts, especially methylammonium iodide (CH_3NH_3I), which has been the basis of rapidly advancing perovskite solar cells, has been made (Fig. 4a). Only with iodide halide was a well-passivated and well-protected surface provided, again one resistant to oxidative attack. As a result, the first photovoltaic-quality n-type CQD inks were recently reported. Quantum junction photovoltaic devices using this new class of CQD ink ascended rapidly to a promising 6% solar power conversion. In late 2015, the most efficient CQD photovoltaics to be processed directly from a fully exchanged ink were reported. These employed the precursors to organometal halide perovskites as ligands, and led in final films to a thin perovskite shell within solid-state CQD films. The crystallized perovskite layer provided a well-passivated and unusually intrinsic quantum dot solid, leading to a PCE of 8.95%[81].

Short organic molecules, such as small hydrophilic mercaptan (≤C3) ligands, have also been explored in preparing CQD inks[82]. 1-thioglycerol (TG) provides colloidal stability in dimethyl sulphoxide. After the phase-exchange ligand-exchange process, during which oleic acid ligands were shown to be removed completely and replaced by TG ligands, the TG ligand was shown to be bound via the sulphur moiety to the CQD surface, and to provide good surface passivation. A further layer of unbound TG ligand helped to stabilize the CQDs through hydrogen bonding in polar solvents, a stabilization mechanism distinct from that at play in the case of

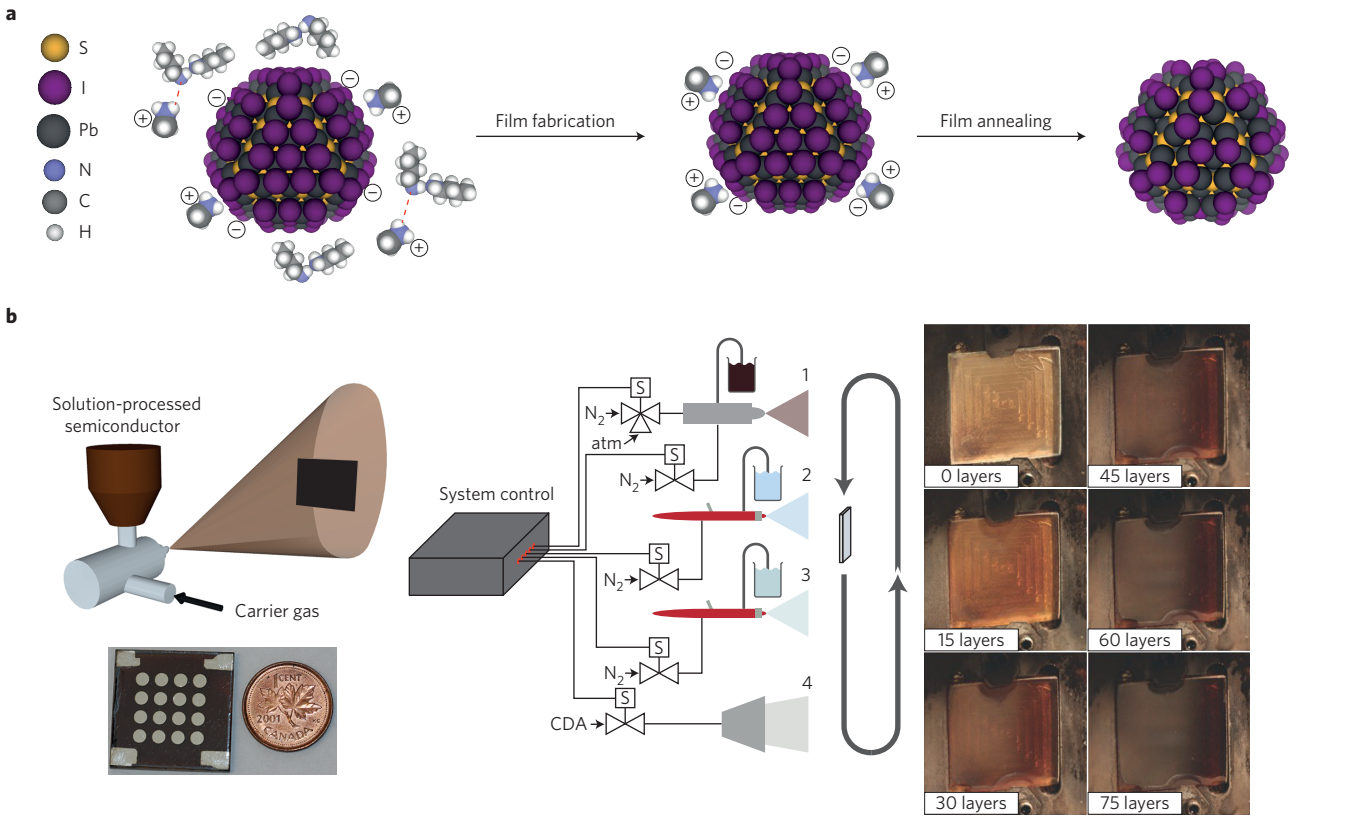

Figure 4 | Advanced materials processing techniques for the scalable manufacturing of CQD solids. a, Solution ligand exchanges to prepare n-type quantum links. The transfer of quantum dots across a phase boundary between nonpolar and polar solvents enables the original organic ligands to be retained in the original nonpolar phase, and the latter is then discarded. The dot-receiving polar phase contains ligands that enable the formation of a stable colloidal dispersion in polar solvents through hydrogen bonds (red dashed lines). **b**, Spray-coating of CQD solids. An automated system was developed to apply quantum dots, ligands in solvent and solvent rinse sequentially. Left panel: sample (black square) mounted in the path of the elliptical spray cross-section. The cone of CQD spray comes out of the spray nozzle. A final device sample after electrode deposition is shown below. Middle panel: full set-up of layer-by-layer spray deposition. Stage one involves the fine mist spraying of CQDs at room atmospheric pressure (atm). Stages two and three use commercial air brushes to spray MPA diluted in methanol and pure methanol, respectively. In stage four, an air blade applies a curtain of high-pressure compressed dry air (CDA) to aid in solvent drying. In all stages, a two-way valve controls carrier gas pressure to the nozzle, whereas in the CQD deposition stage, a three-way valve controls the pilot gas to actuate spraying. All solenoid valves are controlled by a computer through a control-printed circuit board. The looping of the sample through the four stages has been implemented as either a loop in space or in time. Right panel: the resultant devices exhibited enhanced repeatability of performance attributed to the reproducibility of the automated processing combined with the improved purity of the spray-treated films. Figure reproduced from: **a**, ref. 80, American Chemical Society; **b**, ref. 93, Wiley.

inorganic ligands. CQD solar cells based on the organic-capped CQD inks showed initial PCE of 2.1%.

This modest performance was considerably improved through the development of a new and attractive technique for solution-exchanged CQD film formation. Centrifugal casting has been widely employed in the fabrication of composites and ceramics in view of its large scale, low cost and high materials utilization. Until recently it had yet to be deployed in CQD film formation[83]. This was overcome by exchanging to MPA to form a CQD ink in a polar solvent such as dimethylformamide or dimethyl sulphoxide. A substrate was placed in a centrifugation tube filled with the CQD ink and, through the action of centrifugal forces during material casting, solutions containing mixtures of dot sizes were deposited at different rates, leading to a gradient fabricated in a single step[84]. This led to compact and crack-free CQD bandgap-graded films with CQD diameters changed programmably over the vertical extent of the film[85]. The gradient appeared principally in the conduction band, and thus promoted electron extraction, thereby assisting in the extraction of the performance-limiting type of carrier[86–88]. Additionally, the first size-tuned gradient photodiode formed in a single deposition step was reported in this study, and the device exhibited the highest normalized detectivity of any CQD reported, an advance attributed to the gradient-enhanced electric field[89].

Spray coating offers another promising means of large-scale CQD film processing. It is compatible with roll-to-roll processing and has been used to deposit the active layer of photovoltaic devices in other materials systems[90,91]. Until recently, the PCEs of spray-cast devices were low, attributed to poor nano- and microscale morphologies of the active layer[92]. A fully automated spray coater for CQD solar cell fabrication was recently reported[93,94]: a fine mist containing organic-ligand-capped CQDs was deposited on the electrode, and the layer was treated using a crosslinking solution to provide the solid-state place exchange (Fig.4b). This process was repeated several times to achieve the desired thickness. Remarkably, the spray-coating process provided superior average performance compared with conventional spin-coated controls. The inter-particle spacing was found to have been reduced, and minority carriers exhibited 25% greater diffusion length than in spin-coated counterparts[95], consistent with the improved defect density in the spray-cast films. The results reconfirm the importance of CQD film passivation and packing, and of the removal of electronic defects. Large-area, flexible photovoltaic devices were fabricated using this advanced technique. The results re-emphasize the promise of CQDs as a basis for scaling-up solar cell manufacture.

Outlook

The most important task for single-junction CQD solar cells is to continue to press forward to higher and higher efficiencies. CQD technology offers cost advantages over conventional solar cells, and initial studies suggest promise in air-stable operation compared with other emerging thin-film solution-processed technologies; but PCEs of 15% and above must be achieved to become commercially compelling.

The principal path to these further improvements lies in continued reductions in electronic trap state densities. Improving carrier diffusion lengths from their present-day 100–200 nm up to the vicinity of 1 μm (the absorption length on the wings of the excitonic peak) demands further trap state density reductions of two orders of magnitude. The likely short-term path to these improvements will lie in further advances in surface management; and, as these progress, the quality of the bulk of the crystals making up quantum dots may start to limit further trap density reductions, suggesting opportunities for further synthesis optimization, with temperature and reagent purity two key variables worthy of exploration. On a related note, although the polydispersity of quantum dots in a solid — which determines the smoothness of the energy landscape — was recently found not to be a dominant source of voltage loss[85], it could become an influential process once chemical improvement lowers the trap state densities associated with individual dots. For this reason, improvements in control over both monodispersity on synthesis and minimization of aggregation during processing remain parameters deserving refined control.

An exciting frontier in CQD photovoltaics is the integration of these materials as the back (infrared) cell in combination with crystalline silicon, perovskites and organic photovoltaics. Additive improvements to the PCE of up to 20 points have recently been estimated to be available via appropriately size-tuned infrared-bandgap tandem cells[96]. This opportunity invites careful investigation of the faceting, passivation, ligand binding and materials processing of CQD solids having bandgaps in the range of 0.6–1.0 eV.

In the field of innovative materials processing, a major opportunity for convergence has yet to be fully exploited: combining materials chemistry successfully used to define quantum dot superlattices with the best quantum dot, ligand and process combinations needed to make well-passivated solids of high photovoltaic quality. If these currently separate classes of processes could be united, an even higher degree of control over both order and mutual inter-particle surface passivation stands to increase considerably the perfection of the CQD solid.

Received 14 September 2015; accepted 27 January 2016; published 29 February 2016

References

1. Masson, G. *et al. Global Market Outlook for Photovoltaics until 2016* (EPIA, 2012).
2. *Best Research Cell Efficiencies* (NREL, accessed on 11 January 2016); www.nrel.gov/ncpv/images/efficiency_chart.jpg
3. Choi, H., Ko, J., Kim, Y. & Jeong, S. Steric-hindrance-driven shape transistion in PbS quantum dots: understanding size-dependent stability. *J. Am. Chem. Soc.* **135,** 5278–5281 (2013).
4. Smith, D. K., Luther, J. M., Semonin, O. E., Nozik, A. J. & Beard, M. C. Tuning the synthesis of ternary lead chalcogenide quantum dots by balancing precursor reactivity. *ACS Nano* **5,** 183–190 (2011).
5. Moreels, I. *et al.* Composition and size-dependent extinction coefficient of colloidal PbSe quantum dots. *Chem. Mater.* **19,** 6101–6106 (2007).
6. Hwang, G. W. *et al.* Identifying and eliminating emissive sub-bandgap states in thin films of PbS nanocrystals. *Adv. Mater.* **27,** 4481–4486 (2015).
7. Kim, D., Kim, D., Lee, J. & Grossman, J. C. Impact of stoichiometry on the electronic structure of PbS quantum dots. *Phys. Rev. Lett.* **110,** 196802 (2013).
This paper demonstrates the impact of quantum dots' stoichiometry on the electronic structure, indicating how precise control over the stoichiometry in the quantum dots will play an important role in improving the performance of optoelectronic devices.
8. Gai, Y., Peng, H. & Li, J., Electronic properties of nonstoichiometric PbSe quantum dots from first principles. *J. Phys. Chem. C* **113,** 21506–21511 (2009).
9. Zhang, M. *et al.* Charge percolation pathways guided by defects in quantum dot solids. *Nano Lett.* **15,** 3249–3253 (2015).
10. Talapin, D. V. & Murray, C. B. PbSe nanocrystal solids for n- and p-channel thin film field-effect transistors. *Science* **310,** 86–89 (2005).
11. Bozyigt, D., Volk, S., Yarema, O. & Wood, V. Quantification of deep traps in nanocrystal solids, their electronic properties, and their influence on device behavior. *Nano Lett.* **13,** 5284–5288 (2013).
12. Zhitomirsky, D. *et al.* Engineering colloidal quantum dot solids within and beyond the mobility-invariant regime. *Nature Commun.* **5,** 3803 (2013).
13. Bozyigit, D., Lin, W. M. M., Yazdani, N., Yarema, O. & Wood, V. A quantitative model for charge carrier transport, trapping and recombination in nanocrystal-based solar cells. *Nature Commun.* **6,** 6180 (2014).
This paper provides insight into charge transport in different nanocrystal solids and device architectures, essential to understanding the design guidelines for engineering high-performance nanocrystal-based devices.
14. Yoon, W. *et al.* Enhanced open-circuit voltage of PbS nanocrystal quantum dot solar cells. *Sci. Rep.* **3,** 2225 (2013).
15. Zhitomirsky, D., Voznyy, O., Hoogland, S. & Sargent, E. H. Measuring charge carrier diffusion in coupled colloidal quantum dot solids. *ACS Nano* **6,** 5282–5290 (2013).
16. Diaconescu, B., Padilha, L. A., Nagpal, P., Swartzentruber, B. S. & Klimov, V. I. Measurement of electronic states of PbS nanocrystal quantum dots using scanning tunneling spectroscopy: the role of parity selection rules in optical absorption. *Phys. Rev. Lett.* **110,** 127406 (2013).
17. Nagpal, P. & Klimov, V. I. Role of mid-gap states in charge transport and photoconductivity in semiconductor nanocrystal films. *Nature Commun.* **2,** 486 (2011).
18. Bozyigit, D., Jakob, M., Yarema, O. & Wood, V. Deep level transient spectroscopy (DLTS) on colloidal-synthesized nanocrystal solids. *ACS Appl. Mater. Interfaces* **5,** 2915–2919 (2013).
19. Oh, S. J. *et al.* Stochiometric control of lead chalcogenide nanocrystal solids to enhance their electronic and optoelectronic device performance. *ACS Nano* **7,** 2413–2421 (2013).
20. Allgaier, R. S. & Scanlon, W. W. Mobility of electrons and holes in PbS, PbSe and PbTe between room temperature and 4.2 K. *Phys. Rev.* **111,** 1029–1037 (1958).
21. Goodwin, E. D. *et al.* The effects of inorganic surface treatments on photogenerated carrier mobility and lifetime in PbSe quantum dot thin films. *Chem. Phys.* http://dx.doi.org/10.1016/j.chemphys.2015.07.031 (in the press).
22. Bae, W. K. *et al.* Highly effective surface passivation of PbSe quantum dots through reaction with molecular chlorine. *J. Am. Chem. Soc.* **134,** 20160–20168 (2012).
23. Lan, X. *et al.* Passivation using molecular halides increases quantum dot solar cell performance. *Adv. Mater.* **28,** 299–304 (2016).
24. Debnath, R. *et al.* Ambient-processed colloidal quantum dot solar cells via individual pre-encapsulation of nanoparticles. *J. Am. Chem. Soc.* **132,** 5952–5953 (2010).
25. Zhang, J. *et al.* PbSe quantum dot solar cells with more than 6% efficiency fabricated in ambient atmosphere. *Nano Lett.* **14,** 6010–6015 (2014).
26. Ip, A. H. *et al.* Hybrid passivated colloidal quantum dot solids. *Nature Nanotech.* **7,** 577–582 (2012).
This study reports the use of a multiple-liganding strategy that was more effective than a single-ligand approach in eliminating midgap trap states.
27. Thon, S. M. *et al.* Role of bond adaptability in the passivation of colloidal quantum dot solids. *ACS Nano* **7,** 7680–7688 (2013).
28. Tang, J. *et al.* Colloidal-quantum-dot photovoltaics using atomic-ligand passivation. *Nature Mater.* **10,** 765–772 (2011).
29. Ning, Z. *et al.* All-inorganic colloidal quantum dot photovoltaics employing solution-phase-halide passivation. *Adv. Mater.* **24,** 6295–6299 (2012).
30. Niu, G. *et al.* Inorganic halogen ligands in quantum dots: I^-, Br^-, Cl^- and film fabrication through electrophoretic deposition. *Phys. Chem. Chem. Phys.* **15,** 19595–19560 (2013).
31. Zhang, H., Jang, J., Liu, W. & Talapin, D. V. Colloidal nanocrystals with inorganic halide, pseudohalide, and halometallate ligands. *ACS Nano* **8,** 7359–7369 (2014).
32. Dirin, D. N. *et al.* Lead halide perovskites and other metal halide complexes as inorganic capping ligands for colloidal nanocrystals. *J. Am. Chem. Soc.* **136,** 6550–6553 (2014).
33. Woo, J. Y. *et al.* Ultrastable PbSe nanocrystal quantum dots via *in situ* formation of atomically thin halide layers on PbSe(100). *J. Am. Chem. Soc.* **136,** 8883–8886 (2014).
34. Crisp, R. W. *et al.* Nanocrystal grain growth and device architecture for high-efficient CdTe ink-based photovoltaics. *ACS Nano* **8,** 9063–9072 (2014).

35. Goodwin, E. D. *et al.* Effects of post-synthesis processing on CdSe nanocrystals and their solids: correlation between surface chemistry and optoelectronic properties. *J. Phys. Chem. C* **118,** 27097–27105 (2014).
36. Greaney, M. J. *et al.* Controlling the trap state landscape of colloidal CdSe nanocrystals with cadmium halide ligands. *Chem. Mater.* **27,** 744–756 (2015).
37. Brown, P. R. *et al.* Energy level modification in lead sulfide quantum dot thin films through ligand exchange. *ACS Nano* **8,** 5863–5872 (2014).
This paper demonstrates that the absolute energy level of CQDs is critically dependent on surface chemistry. It represents an adjustable parameter in the optimization of CQD-based optoelectronic devices.
38. Soreni-Harani, M. *et al.* Tuning energetic levels in nanocrystal quantum dots through surface manipulations. *Nano Lett.* **8,** 678–684 (2008).
39. Yang, S., Prendergast, D. & Neaton, J. B. Tuning semiconductor band edge energies for solar photocatalysis via surface ligand passivation. *Nano Lett.* **12,** 383–388 (2012).
40. Munro, A. M., Zacher, B., Graham, A. & Armstrong, N. R. Photoemission spectroscopy of tethered CdSe nanocrystals: shifts in ionization potential and local vacuum level as a function of nanocrystal capping ligand. *ACS Appl. Mater. Interfaces* **2,** 863–869 (2010).
41. Jasieniak, J., Califano, M. & Watkins, S. E. Size-dependent valence and conduction band-edge energies of semiconductor nanocrystals. *ACS Nano* **5,** 5888–5902 (2011).
42. Geyer, S. M. *et al.* Control of the carrier type in InAs nanocrystal films by predeposition incorporation of Cd. *ACS Nano* **4,** 7373–7378 (2010).
43. Mocatta, D. *et al.* Heavily doped semiconductor nanocrystal quantum dots. *Science* **332,** 77–81 (2011).
44. Sahu, A. *et al.* Electronic impurity doping in CdSe nanocrystals. *Nano Lett.* **12,** 2587–2594 (2012).
45. Choi, J. *et al.* Bandlike transport in strongly coupled and doped quantum dot solids: a route to high-performance thin-film electronics. *Nano Lett.* **12,** 2631–2638 (2012).
46. Gao, J. *et al.* Quantum dot size dependent J-V characteristics in heterojunction ZnO/PbS quantum dot solar cell. *Nano Lett.* **11,** 1002–1008 (2011).
47. Tang, J. *et al.* Quantum junction solar cells. *Nano Lett.* **12,** 4889–4894 (2012).
This paper reports the first quantum junction diodes based on a single materials synthesis and processing platform. It provides a powerful new degree of freedom in CQD optoelectronics.
48. Voznyy, O. *et al.* Charge–orbital balance picture of doping in colloidal quantum dot solids. *ACS Nano* **6,** 8448–8455 (2012).
49. Scheele, M. *et al.* PbS nanoparticles capped with tetrathiafulvalenetetracarboxylate: utilizing energy level alignment for efficient carrier transport. *ACS Nano* **8,** 2532–2540 (2014).
50. Koh, W. *et al.* Heavily doped n-type PbSe and PbS nanocrystals using ground-state charge transfer from cobaltocene. *Sci. Rep.* **3,** 2004 (2013).
51. Osedach, T. P. *et al.* Bias-stress effect in 1,2-ethanedithiol-treated PbS quantum dot field-effect transistors. *ACS Nano* **6,** 3121–3127 (2012).
52. Engel, J. & Alivisatos, A. P. Postsynthetic doping control of nanocrystal thin films: balancing space charge to improve photovoltaic efficiency. *Chem. Mater.* **26,** 153–162 (2014).
53. Ning, Z. *et al.* Air-stable n-type colloidal quantum dot solids. *Nature Mater.* **13,** 822–828 (2014).
This paper reports the first high-performance, air-stable n-type CQD solids. It provides a platform for active electronics that leverage air-stable quantum-tuned materials.
54. Luther, J. M. *et al.* Stoichiometry control in quantum dots: a viable analog to impurity doping of bulk materials. *ACS Nano* **7,** 1845–1849 (2013).
55. Zhitomirsky, D. *et al.* N-type colloidal-quantum-dot solids for photovoltaics. *Adv. Mater.* **24,** 6181–6185 (2012).
56. Pattantyus-Abraham, A. G. *et al.* Depleted-heterojunction colloidal quantum dot solar cells. *ACS Nano* **4,** 3374–3380 (2010).
57. Luther, J. M. *et al.* Efficient, stable infrared photovoltaics based on a 3% PbS/ZnO quantum dot heterojunction solar cell. *Adv. Mater.* **22,** 3704–3707 (2010).
58. Tang, J. & Sargent, E. H. Infrared colloidal quantum dots for photovoltaics: fundamentals and recent progress. *Adv. Mater.* **23,** 12–29 (2011).
59. Lan, X., Masala, S. & Sargent, E. H. Charge-extraction strategies for colloidal quantum dot photovolatics. *Nature Mater.* **13,** 233–240 (2014).
60. Jean, J. *et al.* ZnO nanowire arrays for enhanced photocurrent in PbS quantum dot solar cells. *Adv. Mater.* **25,** 2790–2796 (2013).
61. Wang, H., Kubo, T., Nakazaki, J., Kinoshita, T. & Segawa, H. PbS-quantum-dot-based heterojunctionsolar cells utilizing ZnO nanowires for high external quantum efficiency in the near-infrared region. *J. Phys. Chem. Lett.* **4,** 2455–2460 (2013).
62. Labelle, A. *et al.* Colloidal quantum dot solar cells exploiting hierarchical structuring. *Nano Lett.* **15,** 1101–1108 (2015).
63. Adachi, M. M. *et al.* Broadband solar absorption enhancement via periodic nanostructuring of electrodes. *Sci. Rep.* **3,** 2928 (2013).
64. Yuan, M., Voznyy, O., Zhitomirsky, D., Kanjanaboos, P. & Sargent, E. H. Synergistic doping of fullerene electron transport layer and colloidal quantum dot solids enhances solar cell performance. *Adv. Mater.* **27,** 917–921 (2014).
65. Choi, J. J. *et al.* Solution-processed nanocrystal quantum dot tandem solar cells. *Adv. Mater.* **23,** 3144–3148 (2011).
66. Liu, H. *et al.* Systematic optimization of quantum junction colloidal quantum dot solar cells. *Appl. Phys. Lett.* **101,** 151112 (2012).
67. Stavrinadis, A. *et al.* Heterovalent cation substitutional doping for quantum dot homojunction solar cells. *Nature Commun.* **4,** 2981 (2013).
68. Rath, A. K. *et al.* Solution-processed inorganic bulk nano-heterojunctions and their application to solar cells. *Nature Photon.* **6,** 529–534 (2012).
69. Rath, A. K., Bernechea, M., Martinez, L. & Konstantatos, G. Solution-processed heterojunction solar cells based on p-type PbS quantum dots and n-type Bi_2S_3 nanocrystals. *Adv. Mater.* **23,** 3712–3717 (2011).
70. Rath, A. K. *et al.* Remote trap passivation in colloidal quantum dot bulk nano-heterojunctions and its effect in solution-processed solar cells. *Adv. Mater.* **26,** 4741–4747 (2014).
71. Ning, Z. *et al.* Graded doping for enhanced colloidal quantum dot photovoltaics. *Adv. Mater.* **25,** 1719–1723 (2013).
72. Yuan, M. *et al.* Doping control via molecularly-engineered surface ligand coordination, *Adv. Mater.* **25,** 5586–5590 (2013).
73. Chuang, C.-H. M., Brown, P. R., Bulovic, V. & Bawendi, M. G. Improved performance and stability in quantum dot solar cells through band alignment engineering. *Nature Mater.* **13,** 796–801(2014).
This paper demonstrates high-performance air-stable quantum dot solar cells through engineering of band alignment at the quantum dot/quantum dot and quantum dot/anode interfaces.
74. Nag, A. *et al.* Metal-free inorganic ligands for colloidal nanocrystals: S^{2-}, HS^-, Se^{2-}, HSe^-, Te^{2-}, HTe^-, TeS_3^{2-}, OH^-, and NH^{2-} as surface ligands. *J. Am. Chem. Soc.* **133,** 10612–10620 (2011).
75. Nag, A., Zhang, H., Janke, E. & Talapin, D. V. Inorganic surface ligands for colloidal nanomaterials. *Z. Phys. Chem.* **229,** 85–107 (2015).
76. Kim, D. K., Lai, Y., Diroll, B. T., Murray, C. B. & Kagan, C. R. Flexible and low-voltage integrated circuits constructed from high-performance nanocrystal transistors. *Nature Commun.* **3,** 1216 (2012).
77. Kovalenko, M. V., Scheele, M. & Talapin, D. V. Colloidal nanocrystals with molecular metal chalcogenide surface ligands. *Science* **324,** 1417–1420 (2009).
This paper demonstrates all-inorganic ligand-capped nanocrystals for highly efficient field-effect transistors.
78. Kovalenko, M. V., Bodnarchuk, M. I., Zaumseil, J., Lee, J. & Talapin, D. V. Expanding the chemical versatility of colloidal nanocrystals capped with molecular metal chalcogenide ligands. *J. Am. Chem. Soc.* **132,** 10085–10092 (2010).
79. Lee, J., Kovalenko, M. V., Huang, J., Chung, D. S. & Talapin, D. V. Band-like transport, high electron mobility and high photoconductivity in all-inorganic nanocrystal arrays. *Nature Nanotech.* **6,** 348–352 (2011).
80. Ning, Z., Dong, H., Zhang, Q., Voznyy, O. & Sargent, E. H. Solar cells based on inks of n-type colloidal quantum dots. *ACS Nano* **8,** 10321–10327 (2014).
81. Yang, Z. *et al.* Colloidal quantum dot photovoltaics enhanced by perovskite shelling. *Nano Lett.* **15,** 7539–7543 (2015).
82. Fischer, A. *et al.* Directly deposited quantum dot solids using a colloidally stable nanoparticle ink. *Adv. Mater.* **25,** 5742–5749 (2013).
83. Kim, J. Y. *et al.* Single-step fabrication of quantum funnels via centrifugal colloidal casting of nanoparticle films. *Nature Commun.* **6,** 7772 (2015).
84. Carney, R. P. *et al.* Determination of nanoparticle size distribution together with density or molecular weight by 2D analytical ultracentrifugation. *Nature Commun.* **2,** 335 (2011).
85. Zhitomirsky, D. *et al.* Colloidal quantum dot photovoltaics: the effect of polydispersity. *Nano Lett.* **12,** 1007–1012 (2012).
86. Jasieniak, J., Califano, M. & Watkins, S. E. Size-dependent valence and conduction band-edge energies of semiconductor nanocrystal. *ACS Nano* **5,** 5888–5902 (2011).
87. Xu, F. *et al.* Efficient exciton funneling in cascaded PbS quantum dots superstructures. *ACS Nano* **5,** 9950–9957 (2011).
88. Kramer, I. J., Levina, L., Debnath, R., Zhitomirsky, D. & Sargent, E. H. Solar cells using quantum funnels. *Nano Lett.* **11,** 3701–3706 (2011).
89. Konstantatos, G. *et al.* Hybrid graphene–quantum dot phototransistors with ultrahigh gain. *Nature Nanotech.* **7,** 363–368 (2012).
90. Nie, W. *et al.* High efficiency organic solar cells with spray coated active layers comprised of a low band gap conjugated polymer. *Appl. Phys. Lett.* **100,** 083301 (2012).
91. Akhavan, V. A. *et al.* Spray-deposited $CuInSe_2$ nanocrystal photovoltaics. *Energy Environ. Sci.* **3,** 1600–1606 (2010).

92. Genovese, M. P., Lightcap, I. V. & Kamat, P. V. Sun-believable solar paint. A transformative one-step approach for designing nanocrystalline solar cells. *ACS Nano* **5,** 865–872 (2011).
93. Kramer, I. J. *et al.* Efficient spray-coated colloidal quantum dot solar cell. *Adv. Mater.* **27,** 116–121 (2015).
94. Kramer, I. J., Moreno-Bautista, G., Minor, J. C., Kopilovic, D. & Sargent, E. H. Colloidal quantum dot solar cells on curved and flexible substrates. *Appl. Phys. Lett*. **105,** 163902 (2014).
95. Kramer, I. J. & Sargent, E. H. The architecture of colloidal quantum dot solar cells: materials to devices. *Chem. Rev.* **114,** 863–882 (2014).
96. Ip, A. H. *et al.* Infrared colloidal quantum dot photovoltaics via coupling enhancement and agglomeration suppression. *ACS Nano* **9,** 8833–8842 (2015).

Acknowledgements

This publication is based in part on work supported by Award KUS-11-009-21 made by King Abdullah University of Science and Technology; by the Ontario Research Fund Research Excellence Program; and by the Natural Sciences and Engineering Research Council of Canada.

Additional information

Reprints and permissions information is available online at www.nature.com/reprints. Correspondence should be addressed to E.H.S.

Competing interests

The authors declare no competing financial interests.